The Geometry of Separation Boundaries. II. Mathematical Formalism

Angelo Lucia
Dept. of Chemical Engineering, University of Rhode Island, Kingston, RI 02881

Ross Taylor
Dept. of Chemical and Biomolecular Engineering, Clarkson University, Potsdam, NY 13699

DOI 10.1002/aic.11204
Published online May 14, 2007 in Wiley InterScience (www.interscience.wiley.com).

This article is concerned with the mathematical proof that distillation boundaries correspond to locally longest residue curves. Perturbation theory and the implicit function theorem are used to provide an analytical relationship between neighboring trajectories while local congruence and a variety of limiting arguments are used to establish the relative distances between neighboring residue curves. The mathematical conditions on which this analysis is based include (1) The assumptions that trajectories are twice continuously differentiable and do not cross. (2) The comparison of neighboring trajectories that converge to the same *stable node. (3) The existence and placement of a proper focal point. (4) Local congruence. While all of these assumptions and conditions are important, it is the existence and proper placement of a focal point and local congruence that are the keys to establishing relative distances between neighboring residue curves and, in turn, the main result that distillation boundaries are defined by locally longest trajectories from any unstable node to all reachable stable nodes. Wherever possible, geometric illustrations are used to clarify key concepts.* © 2007 American Institute of Chemical Engineers *AIChE J,* 53: 1779–1788, 2007

Introduction

Residue curves are an important tool in understanding the synthesis, design, and operation of separation processes. They have a long history (see, Ostwald[1,2]; Scheinermakers[3–5]] and have been successfully applied to azeotropic distillation, reactive separations, and crystallization. See, for example, the work of Doherty and coworkers (Barbosa and Doherty[6–8]; Pham and Doherty[9,10]; Slaughter and Doherty[11]] as well as that of Fien and Liu,[12] Peterson and Partin,[13] and others. For mixtures that exhibit azeotropic or eutectic points, separation boundaries can occur and these boundaries can limit the degree of separation that can be achieved by open evaporation or condensation. Therefore, correct synthesis and design of many separations requires correct knowledge of the location and shape of these boundaries. Rooks et al.[14] determine separation boundaries using a method based on calculating the eigenstructure of the matrix $[J_{yx} - I]$ at saddle points, where J_{yx} is the (c-1) × (c-1) matrix of first partial derivatives of vapor composition with respect to liquid composition and c is the number of components in the mixture. Pöpken and Gmehling[15] apply the method of Rooks et al. to four component mixtures, which are typical in reactive separations.

Recently, Lucia and Taylor[16] have adopted a very different approach and have presented a novel geometric characterization of separation boundaries in terms of line integrals, surface areas, and volumes. In particular, Lucia and Taylor show that separation boundaries for ternary azeotropic liquid mixtures can be characterized as local maxima in the line integral from any unstable node to all reachable stable nodes. The key concept in this approach is to view a boundary as

Correspondence concerning this article should be addressed to A. Lucia at lucia@egr.uri.edu

an integral curve that runs from an unstable node to a stable node, and not to interpret a boundary as a trajectory that stops at a saddle point. Moreover, it is important to understand that it is only from this perspective that separation boundaries correspond to local maxima in line integrals for ternary mixtures. This is illustrated in Figure 1 for the ternary mixture chloroform, acetone and benzene at 1 atm. In the context of our geometric approach, the separation boundary shown in Figure 1 runs from the unstable benzene node with respect to $x' = y - x$ to the pure acetone and pure chloroform vertices, which are both stable nodes. It does not terminate at the chloroform/acetone azeotrope or the saddle point. Here x denotes liquid composition and y corresponds to the composition of the vapor. In addition, the portion of separation boundary that is internal to the triangular feasible region (i.e., the part that the runs from the benzene vertex to the chloroform/acetone azeotrope) is easily extracted from these maximum line integrals.

Lucia and Taylor also describe the wide applicability of their approach to mixtures with four or more components by using surface areas and volumes in place of line integrals, to reactive and nonequilibrium separations, and to other separation processes like crystallization. Recently, Bellows and Lucia[17] present theory, algorithms, and numerical results that show that separation boundaries in four component mixtures are local maxima in surface area subject to Levi-Civita parallelism.

The purpose of this article is to present a mathematical formalism for this new geometric approach to separation boundaries. Accordingly, the geometric method of Lucia and Taylor[16] is summarized and followed by some preliminary geometric discussions for ternary homogeneous liquid mixtures. The main contribution of this article, rigorous proof that separation boundaries for ternary mixtures are local maxima in line integrals, is next. The article ends with a summary of the important aspects of this article and some indication of future study.

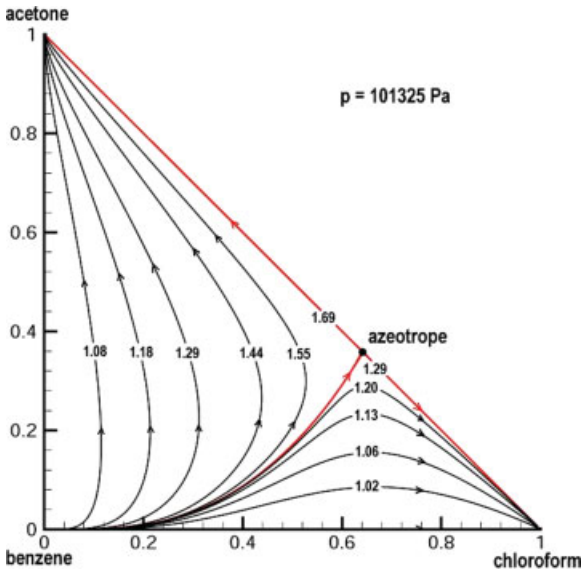

Figure 1. Residue curve map and line integrals for chloroform/acetone/benzene.

[Color figure can be viewed in the online issue, which is available at www.interscience.wiley.com.]

A geometric methodology of separation boundaries

Lucia and Taylor[16] define a separation boundary for any ternary mixture as the trajectory, say $x^*(\alpha)$, associated with the solution of the nonlinear programming problem

$$\max_{x(0)} \quad D = \int_0^T \|x'(\alpha)\| d\alpha \tag{1}$$

$$\text{subject to} \quad x'(\alpha) = y[x(\alpha)] - x(\alpha) \tag{2}$$

$$x(T) = x_T \tag{3}$$

where D represents a line integral or distance function along a trajectory, $\|.\|$ denotes the two-norm, $x(0)$ is any feasible set of initial conditions on the ball (or circle in the case of a ternary mixture) of radius ε about some designated unstable node x_0, and x_T is a stable node. The ball of radius ε about a designated unstable node, x_0, is defined by $B(x_0, \varepsilon) = \{x: \|x - x_0\| = \varepsilon \text{ for all } x\}$ and it is important to note that the objective function, D, in Eq. 1 is only a function of the initial conditions, $x(0)$, which are the unknown optimization variables. Thus any trajectory, $x^*(\alpha)$, that corresponds to a local maximum value of the line integral is a separation boundary. Note that in theory this trajectory, $x^*(\alpha)$, can pass directly through a saddle point and then split or bifurcate and continue to two different stable nodes as depicted in Figure 1. That is, the portion of the separation boundary in Figure 1 from the benzene vertex to the saddle point chloroform-acetone azeotrope is in theory a single curve that subsequently splits and goes to both the pure chloroform and pure acetone vertices. In practice, however, the portion of the separation boundary that runs from the benzene vertex to the chloroform–acetone azeotrope will actually be two distinct but essentially coincident trajectories that turn away from each other very close to the chloroform–acetone azeotrope.

Mathematical preliminaries

To better understand our geometric framework, it is necessary to establish a rigorous understanding of just what is meant by a separation boundary and the mathematical formalism that accompanies this definition.

Separation boundaries

It is long been known that any residue curve given by

$$x' = y(x) - x \tag{4}$$

is a deterministic set of c-1 ordinary differential equations whose behavior is completely defined by specifying initial conditions $x(0)$. Here we let x be the liquid composition and y be the composition of any incipient phase (i.e., solid or vapor). The fixed points of the residue curve given in Eq. 4 are the pure component vertices and the azeotropic or eutectic points and these fixed points can be stable or unstable nodes or saddle points. See, for example, p. 285 in Doherty and Perkins.[18] Moreover, a collection of residue curves is called a residue curve map and trajectories run from unstable nodes to stable nodes. We note here that in a strict numerical

sense, trajectories do not leave exactly from an unstable node. They only truly move from a neighborhood (i.e., feasible $x(0)$ on $B(x_0, \varepsilon)$) surrounding an unstable node to a stable node. Moreover, how close trajectories get to the stable node can also be a function of finite length arithmetic and imposed convergence tolerances. However, these issues present no theoretical consequences in measuring line integrals since we can always assume infinite precision and that $\varepsilon > 0$ is infinitesimal. We also know from the work of Doherty and Perkins[18] that trajectories do not cross. Finally, we remark that it is customary to write residue curves in the form $x' = x - y(x)$, where the flow of trajectories is from low to high temperature. However, in this work we have chosen to write residue curve as shown in Eq. 4; thus the flow of trajectories is from high to low temperature. Each form is correct and is simply a matter of choice.

It is convenient to use spherical coordinates and to define initial conditions through the ball of radius ε, $B(x_0, \varepsilon)$. Feasible initial conditions for any ternary mixture can be defined by

$$x(0) = x_0 + \varepsilon[\cos\theta, \sin\theta] \quad \text{for } \theta_{\min} \le \theta \le \theta_{\max}, \tag{5}$$

where $\theta_{\min}$ and $\theta_{\max}$ are minimum and maximum values of the rotation angle, θ, that enforce feasibility on x. Thus given ε, each value of θ corresponds to a unique $x(0)$. Moreover, there is a unique trajectory, $x(\alpha)$, and corresponding distance, D defined by Eq. 1, for each θ, which clearly follows from fundamental existence and uniqueness theorems of differential equations (see, for example, Hurewicz[19]).

Perturbation analysis

Since trajectories are uniquely determined by initial conditions, we can use continuity and the implicit function theorem to relate neighboring residue curves in a quantitative way— provided we assume some degree of continuous differentiability. First, Eq. 5 clearly shows that $x(0)$ is a function of ε and θ. For fixed e

$$\Delta x(0) = \varepsilon[-\sin\theta, \cos\theta]\Delta\theta \tag{6}$$

Note we have denoted any change in initial conditions by the symbol $\Delta x(0)$ so as not to confuse it with the stable node x_0. Also, the use of forward Euler's method for the integration of Eq. 4 gives $x_{k+1} = x_k + h[y_k - x_k]$, which can easily be re-written in the form $F(x_{k+1}, x_k) = x_k + h[y_k - x_k] - x_{k+1} = 0$, where h is an integration step size and k is an integration step counter. Application of the implicit function theorem (Taylor and Mann[20]) to $F(x_{k+1}, x_k) = 0$ gives

$$\Delta x_{k+1} = J_k \Delta x_k \tag{7}$$

where $J_k = I + h[J_{yx} - I]$ and where J_{yx} is the (c-1) $\times$ (c-1) Jacobian matrix of y with respect to x and contains the implicit effects of temperature derivatives with respect to x as well as the summation equation for y. It is important to understand that the functionality given by Eq. 7 accumulates over the integration process. That is, $\Delta x_1 = J_0 \Delta x(0)$, $\Delta x_2 = J_1 \Delta x_1 = J_1 J_0 \Delta x(0)$, and so on. Consequently, from any $\Delta x(0)$ that corresponds to two separate initial values on $B(x_0, \varepsilon)$, we have that

$$\Delta x_{k+1} = \left\{ \prod_{i=0}^{k-1} \mathrm{J}_i \right\} \Delta x(0), \quad k = 1, \ldots, N \tag{8}$$

where N is some number of integration steps. Furthermore, using Eq. 6 we can write Eq. 8 in terms of changes in the rotation angle $\Delta\theta$. That is,

$$\Delta x_{k+1} = \left\{ \prod_{i=0}^{k-1} \mathrm{J}_i \right\} \varepsilon[-\sin\theta, \cos\theta]\Delta\theta, \quad k = 1, \ldots, N. \tag{9}$$

With these equations established it is straightforward to see that perturbations in initial values on $B(x_0, \varepsilon)$ propagate along any trajectory. Thus given a base trajectory, say $x_1(\alpha)$, we can determine the quantitative shape of a neighboring trajectory, $x_2(\alpha)$—or vice versa—as a function of $\Delta\theta$. Moreover, in the limit as $\Delta\theta$ goes to zero these neighboring trajectories will be one and the same. We write the limiting value of $\Delta\theta$ as the infinitesimal quantity $\mathrm{d}\theta$. This allows us to come to some agreement on what exactly is meant by separation boundaries. We restrict our attention to ternary mixtures for the remainder of this article. We recommend that the reader frequently refer back to this section on perturbation analysis in building an understanding of the limiting arguments in subsequent sections.

Definition of separation boundaries

Let $\varepsilon > 0$ be given and let $x(\alpha^*)$ be the trajectory of $x' = y - x$ associated with θ^* such that $\theta_{\min} \le \theta^* \le \theta_{\max}$. Then $x(\alpha^*)$ is a separation boundary if for any $\mathrm{d}\theta$, the initial conditions, $x_1(0)$ and $x_2(0)$, and the trajectories, $x_1(\alpha)$ and $x_2(\alpha)$, of $x' = y - x$ associated with $(\theta^* + \mathrm{d}\theta)$ and $(\theta^* - \mathrm{d}\theta)$ respectively satisfy one of the following conditions:

(1) $x_1(\alpha)$ and $x_2(\alpha)$ are feasible and converge to different stable nodes.
(2) Either $x_1(0)$ or $x_2(0)$ is infeasible.

Condition 1 is straightforward and its meaning can be interpreted using Figure 1 by considering the curve that denotes the separation boundary in this case. Here $\theta^* = 3.829310180 \times 10^{-11}$ radians and perturbation $\mathrm{d}\theta > 0$ from θ^* results in a trajectory that converges to the acetone vertex while the perturbation $-\mathrm{d}\theta$ converges to the chloroform vertex. Because all trajectories run from an unstable to a stable node, we must also allow for the possibility that part or all of a separation boundary corresponds to an edge of the triangular region. For example, suppose the azeotrope in Figure 1 was a minimum boiling azeotrope. In this situation, the benzene vertex would remain as the only unstable node, the chloroform and acetone vertices would become saddle points, and the minimum boiling azeotrope would become the only stable node with respect to $x' = y - x$. As a result, there would be two trajectories of local maximum length corresponding to $\theta_1^* = 0$ and $\theta_2^* = \pi/2$, and the resulting separation boundaries in our geometric framework would be the edges of the triangular region. However, note that feasibility about the benzene vertex is constrained and implies that $0 \le \theta \le \pi/2$. Therefore both locally optimal rotation angles lie on the boundary of the feasible region. Consequently, perturbation from either θ_1^* or θ_2^* is only feasible in one direction, either $\mathrm{d}\theta > 0$ or $\mathrm{d}\theta < 0$. This is the reason for

condition 2. An alternative way of stating condition 2 is to say that $x(\alpha^*)$ is a separation boundary if there is only a one-sided perturbation $d\theta$ such that the resulting trajectory is feasible and converges to a given stable node.

The local congruence of neighboring residue curves

Here we use the fact that residue curves do not cross to establish a local geometric congruence relationship between neighboring residue curves whose initial conditions differ by an infinitesmal amount $d\theta$. Consider Figure 2, which has been exaggerated for the purpose of clarity.

In this figure, we let the trajectories, $x_1(\alpha)$ and $x_2(\alpha)$, in each separation region represent two neighboring trajectories whose initial conditions differ by $d\theta$ with respect to $B(x_0, \varepsilon)$. Also shown in Figure 2 are two rays, r_1 and r_2, that both emerge from some focal point, z, and whose angle between them is $d\omega$. Ray r_1 intersects trajectories, $x_1(\alpha)$ and $x_2(\alpha)$, at points a_1 and b_1, respectively while ray r_2 intersects the same two trajectories at points a_2 and b_2, respectively. The rays r_1 and r_2 are constructed in such a way that each intersects the trajectories $x_1(\alpha)$ and $x_2(\alpha)$ once. However, this is for illustrative purposes only and is not a condition that is necessary for the subsequent proofs to be valid. Finally, the lines connecting a_1' and a_2' and b_1' and b_2' represent the average of the slopes at the mean values c_1' and c_2' and are also depicted in Figure 2. Thus the lines connecting a_1' and a_2' and b_1' and b_2' have exactly the same slope as $d\theta$ and $d\omega$ go to zero. We note that the illustrated focal points shown in Figure 2 are outside the triangular region. However, focal points can occur inside the triangular region as well.

The gist of the geometric arguments here are as follows. For two initial values, $x_1(0)$ and $x_2(0)$, in the same separation region that are differentially close, the shapes of the resulting trajectories are essentially the same. This follows from the continuity of Eq. 4 with respect to initial conditions. However, because trajectories do not cross, one curve, say $x_2(\alpha)$, must always lie further away from a focal point, z, than the other, $x_1(\alpha)$, as measured along any ray emerging from z. Therefore, if we consider the portions of these neighboring trajectories that lie between the pair of rays, r_1 and r_2, as $d\omega$ goes to 0, the distances along $x_1(\alpha)$ and $x_2(\alpha)$ between the rays approach the distances along the straight lines $a_1'a_2'$ and $b_1'b_2'$. Moreover, these straight lines are parallel and approach the (tangents of the) true curves a_1a_2 and b_1b_2 respectively as $x_1(0)$ and $x_2(0)$ get closer to each other or as $d\theta$ goes to zero. As a result, the two regions defined by $za_1'a_2'$ and $zb_1'b_2'$ form locally congruent triangles and it follows that $\| b_1'b_2' \| > \| a_1'a_2' \|$. Moreover, in the limit as $d\theta$ and $d\omega$ go to 0, this implies that $\| b_1b_2 \| > \| a_1a_2 \|$.

To extend this analysis to the full length of $x_1(\alpha)$ and $x_2(\alpha)$ we can repeatedly apply the same local congruence arguments over adjacent pairs of rays, say r_1–r_2, r_2–r_3, ..., with differential angles $d\omega$ between them until we cover exactly all of both trajectories, $x_1(\alpha)$ and $x_2(\alpha)$, from unstable to stable node. However, before we can do this we must also establish two other important and interrelated facts:

(1). The existence and location of the focal point, z,
(2). Measurement of distance near the unstable and stable node.

Focal points

It is by no means obvious that the focal point, z, exists or that it provides a means of correctly measuring distances along entire trajectories. As we show shortly, focal points that lead to correct distance measurements can always be selected and that the correct location of any focal point is related to the manner in which distances must be measured near the unstable and stable node.

Distances near nodes

Note that local congruence arguments cannot be used to measure distance near the endpoints of trajectories since each pair of trajectories, in theory, emerges from and converges to the same exact point (i.e., the unstable and stable nodes). See Figure 3. Regardless of the radius of the ball around each of the nodes, one can never show that the triangles, $za_{10}a_{11}$ and $zb_{10}b_{11}$, or the triangles, $za_{1N\text{-}1}a_{1N}$ and $zb_{1N\text{-}1}b_{1N}$, form pairs of congruent triangles in the limit. To resolve this difficulty we must find a different way to accurately measure distances near nodes. Therefore, consider the ball, $B(x_0, \varepsilon_0)$ shown in Figure 3 and remember, the discussions here are for illustrative purposes. Note that $x_0 = a_{10} = b_{10}$ and that $x_1(0) = a_{11}$ and $x_2(0) = b_{11}$ or that the initial conditions for each trajectory lie on the ball of radius ε_0 about the unstable node. Moreover, feasibility requires that any line connecting $x_1(0) = a_{11}$ and $x_2(0) = b_{11}$ must have a slope that is negative with a value bounded between minus infinity and zero. Therefore this line connecting $x_1(0)$ and $x_2(0)$ is unique and must move toward the vertical axis of the triangular region shown in Figure 3. As a result, it is always possible to choose a value of $\varepsilon_0 > 0$ such that an extension of this line (i.e., the ray r_1) crosses the vertical axis before it reaches the

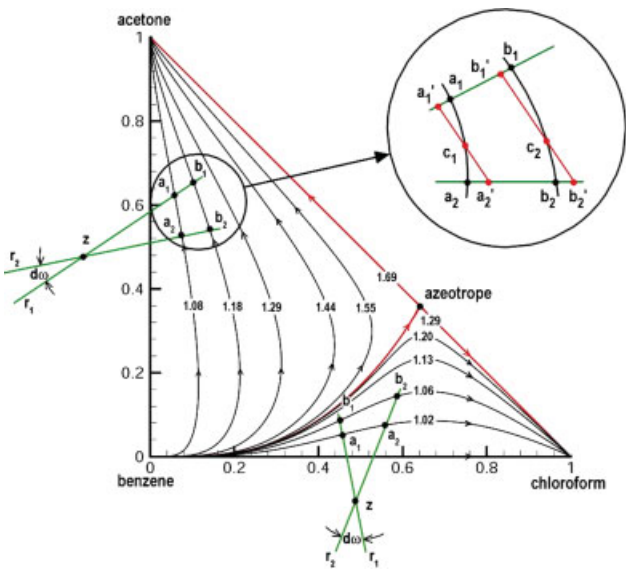

Figure 2. Local congruence of neighboring residue curves.

[Color figure can be viewed in the online issue, which is available at www.interscience.wiley.com.]

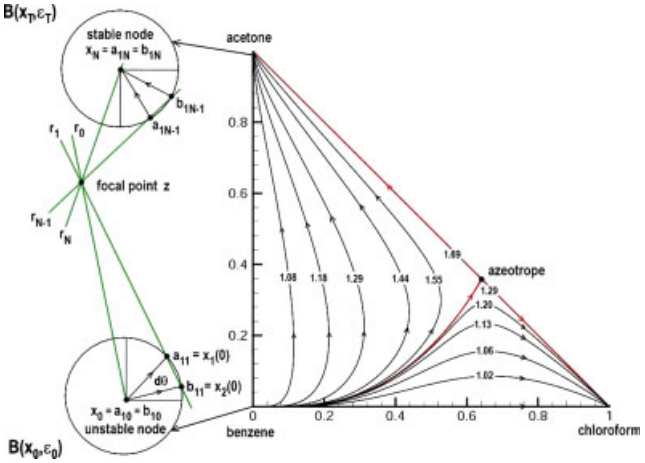

Figure 3. A focal point for neighboring residue curves.

[Color figure can be viewed in the online issue, which is available at www.interscience.wiley.com.]

acetone vertex. This value ε_0 may be quite small but nonetheless it must be nonzero since the slope of the ray r_1 can never be exactly minus infinity. Independent of this, we can also always choose a value of the radius of a ball around the stable node, $B(x_T, \varepsilon_T)$, such that $\varepsilon_T > 0$.

In addition, we are free to rotate the ray r_{N-1} by keeping the point b_{1N-1} fixed in such a way that the slope of the ray r_{N-1} is positive and bounded above by infinity and such that the point a_{1N-1} is either on or inside $B(x_T, \varepsilon_T)$ and still on the trajectory $x_1(\alpha)$. Since r_1 and r_{N-1} can be chosen in a way that they do not have the same slope, it follows that their intersection (i.e., the focal point z) exists and provides a means of measuring distance. Furthermore, these conditions guarantee that the distance along the part of any trajectory within $B(x_0, \varepsilon_0)$ is ε_0 and the distance along the part of any trajectory within $B(x_T, \varepsilon_T)$ is less than or equal to ε_T. However, we caution the reader about concluding that the focal point is unique; it's not! Because we are free to rotate the ray r_{N-1}, there are an infinite number of focal points that can be used to measure distance. It is also important to caution the reader to be careful about concluding that the ray r_{N-1} can be pivoted about the point a_{1N-1} (instead of b_{1N-1}). It cannot without resulting in ambiguities associated with the relative distances of neighboring trajectories. In particular, it voids the necessary conditions around the unstable node that $a_{1N-1}a_{1N} < \varepsilon_T$ and $b_{1N-1}b_{1N} = \varepsilon_T$, which are required to prove the main result.

Although the foregoing discussion of measuring distances near nodes is specific to Figure 3 certain characteristics hold in general. These include the facts that

(1). Initial conditions $x_1(0)$ and $x_2(0)$ must lie on $B(x_0, \varepsilon_0)$.
(2). Distances of all trajectories from x_0 to $B(x_0, \varepsilon_0)$ are equal to ε_0.
(3). Ray r_1 is uniquely determined by initial conditions $x_1(0)$ and $x_2(0)$ and thus its slope is fixed.
(4). We are free to choose N as large as desired.
(5). Using rotation, the ray r_{N-1} can be chosen such that its slope is different from that of r_1.
(6). Correct rotation of r_{N-1} means the distance $a_{1N-1}a_{1N}$ is bounded above by ε_T.
(7). Fixing the slope of r_1 limits the possible locations of the focal point and provides proper placement of z.
(8). The remaining rays r_0, r_2, r_3, …, r_{N-2}, and r_N are easily placed once z is known.

These facts now permit us to make the following strong statement about the behavior of neighboring residue curves. However, before proving the main theorems in this article we note that it is also possible to analyze distances near nodes by making use of the fact that all trajectories approach (or leave) a node along the direction associated with the smallest eigenvalue of the matrix $[J_{yx} - I]$. Nonetheless, the inserts in Figure 3 and the accompanying mathematical reasoning also apply to this situation under suitable enlargement (or length scale) and thus the foregoing results regarding distances near nodes remain unchanged.

Theorem 1. *Let $x_1(\alpha)$ and $x_2(\alpha)$ be neighboring trajectories associated with $x' = y - x$ for a given pair of unstable and stable nodes, x_0 and x_T. Moreover let the initial conditions, $x_1(0)$ and $x_2(0)$, associated with $x_1(\alpha)$ and $x_2(\alpha)$ respectively differ by $d\theta$ for some $B(x_0, \varepsilon_0)$, where $\varepsilon_0 > 0$. Then it follows that $D_2 > D_1$, where D is defined by*

$$D = \int_0^T \|x'(\alpha)\| \mathrm{d}\alpha \tag{10}$$

Proof. Using the facts just established, we can choose $\varepsilon_0 > 0$, $\varepsilon_T > 0$ and r_{N-1} such that the following are true:

(1). There exists a focal point, z.
(2). The distance from $x_1(0)$ and $x_2(0)$ to x_0 is exactly ε_0.
(3). The distance from any point on $B(x_T, \varepsilon_T)$ to x_T is $<\varepsilon_T$.

Let N be a sufficiently large positive integer. The initial values, $x_1(0)$ and $x_2(0)$, lie on $B(x_0, \varepsilon_0)$ and provide a unique slope for r_1 while we are free to pivot r_{N-1} so that a focal point z can be established. Once z is determined, the rays r_0 and r_N, as shown in Figure 3, are also determined. Moreover adjacent rays r_2, r_3,…, r_{N-2} that also emerge from the focal point, z, can be constructed in such a way that the angle between them is $d\omega$ and such that each ray intersects $x_1(\alpha)$ and $x_2(\alpha)$ respectively exactly once at a_{21}, b_{21}, a_{31}, b_{31}, and so on, respectively. See Figure 4. Using the arguments that were presented earlier, it follows that there are limiting congruent triangles $za_{11}a_{21}$ and $zb_{11}b_{21}$ such that $\| b_{11}b_{21} \| > \|a_{11}a_{21}\|$. Repeating these arguments for successive pairs of rays gives

$$\|b_{1j}b_{2j}\| > \|a_{1j}a_{2j}\| \quad \text{for each } j = 1, \ldots, N-1 \tag{11}$$

where $x_0 = a_{10} = b_{10}$ and $x_T = a_{1N} = b_{1N}$ denote the unstable and stable node, respectively. However, Eq. 11 implies that

$$\sum_{j=1}^{N-1} \|b_{1j}b_{2j}\| > \sum_{j=1}^{N-1} \|a_{1j}a_{2j}\| \tag{12}$$

All that remains is to resolve the distances near the nodes along each trajectory. Using facts 2 and 3, it follows that $a_{10}a_{11} = b_{10}b_{11} = \varepsilon_0$ while the distance $a_{1N-1}a_{1N} <\varepsilon_T$ and

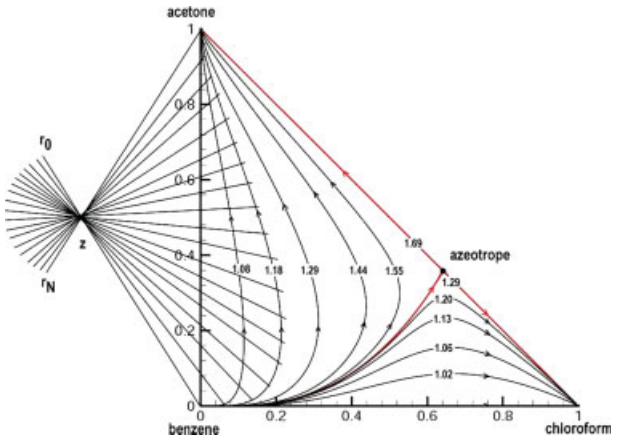

Figure 4. Distances along neighboring residue curves.

[Color figure can be viewed in the online issue, which is available at www.interscience.wiley.com.]

$b_{1N\text{-}1}b_{1N} = \varepsilon_T$. This, in turn, implies that

$$\sum_{j=0}^{N} \|b_{1j}b_{2j}\| = \sum_{j=1}^{N-1} \|b_{1j}b_{2j}\| + \varepsilon_0 + \varepsilon_T$$

$$> \sum_{j=1}^{N-1} \|a_{1j}a_{2j}\| + \varepsilon_0 + \varepsilon_T > \sum_{j=0}^{N} \|a_{1j}a_{2j}\| \quad (13)$$

In the limit as $d\omega$ goes to 0, $\Sigma\|a_{1j}a_{2j}\| = \int \|x_1'(\alpha)\|d\alpha = D_1$ and $\Sigma \|b_{1j}b_{2j}\| = \int \|x_2'(\alpha)\|d\alpha = D_2$, and $D_2 > D_1$.

Remarks

To understand Theorem 1 the reader must understand the various limiting arguments needed to establish relative distances of trajectories. First, any pair of trajectories can be forced closer and closer together (but can never cross) by letting $d\theta$ go to zero. Second, the slope of the ray r_1 is unique, fixed, and a simple consequence of feasibility and the fact that initial conditions for pairs of trajectories are deliberately chosen to lie on $B(x_0, \varepsilon_0)$. Reducing ε_0 does not change these facts. The choice of $\varepsilon_T > 0$, which is independent of ε_0, allows distances along $x_1(\alpha)$ and $x_2(\alpha)$ within $B(x_T, \varepsilon_T)$ to be bounded above by ε_T. Furthermore, the intersection of $B(x_T, \varepsilon_T)$ with $x_1(\alpha)$ and $x_2(\alpha)$ and the freedom to rotate $r_{N\text{-}1}$ establishes an appropriate slope of the ray, $r_{N\text{-}1}$. Together the rays r_1 and $r_{N\text{-}1}$ establish the existence of a correctly placed focal point, z. Incorrect placement of z will result in $a_{1N\text{-}1}a_{1N} > b_{1N\text{-}1}b_{1N}$, which voids Eq. 13 and means that no definitive conclusions can be made with regard to which trajectory, $x_1(\alpha)$ or $x_2(\alpha)$ is longest. Third and independent of this, by letting $d\theta$ and $d\omega$ go to zero, the neighboring trajectories $x_1(\alpha)$ and $x_2(\alpha)$ can then be divided into a sufficiently large number of rays (shown as r_0 through r_N in Figure 4) for local congruence to apply in the limit. Fourth, nothing that we have illustrated using Figures 2, 3, and 4 is actually specific to the particular ternary mixture or the relative location of stable and unstable nodes. The results apply to ternary mixtures in general. Finally, the significance of Theorem 1 is that this theorem, together with the definition of separation boundaries given earlier, establishes a way to show that separation boundaries for ternary mixtures correspond to local maxima in line integrals.

The equivalence of separation boundaries and local maxima in line integrals

In this section, we establish that separation boundaries for ternary mixtures can be characterized by local maxima in line integrals. To do this, we use the results of Theorem 1 and the definition of a separation boundary established earlier in this manuscript.

Theorem 2. *The trajectory $x(\alpha^*)$ associated with $x' = y - x$ is a separation boundary if and only if it is a local maximum in the line integral.*

Proof. First assume that $x(\alpha^*)$ is a separation boundary. From the definition of a separation boundary, it follows that there exists a one-sided perturbation (i.e., either $d\theta > 0$ or $d\theta < 0$) such that $x(\alpha)$ is feasible and converges to the desired stable node, x_T. Set $x_1(\alpha) = x(\alpha)$ and $x_2(\alpha) = x(\alpha^*)$ such that the initial conditions, $x_1(0)$ and $x_2(0)$, associated with $x_1(\alpha)$ and $x_2(\alpha)$ respectively differ by $d\theta$ for some $B(x_0, \varepsilon_0)$, where $\varepsilon_0 > 0$. Then by Theorem 1 there exists a focal point z such that $D_2 > D_1$. Moreover, because $d\theta$ is a one-side perturbation, it follows that D_2 is a local maximum.

Of course, we could have just as easily set $x_1(\alpha) = x(\alpha^*)$ and $x_2(\alpha) = x(\alpha)$. However, this choice of $x_1(\alpha)$ and $x_2(\alpha)$ has no real consequence since then we can show that $D_1 > D_2$ by adjusting the arguments related to Theorem 1 to correctly reflect the neighboring trajectories.

Assume $x(\alpha^*)$ corresponds to a local maximum in the line integral with associated rotation angle θ^*. Also let D^* be the value of the line integral along $x(\alpha^*)$. Suppose that $x(\alpha^*)$ is not a separation boundary. Since $x(\alpha^*)$ is not a separation boundary, there exists a two-sided perturbation $d\theta$ such that the corresponding trajectory $x(\alpha)$ is feasible and converges to the desired stable node. Moreover, at least one perturbation $d\theta > 0$ or $d\theta < 0$ must result in a trajectory, say $x_1(\alpha)$ or $x_2(\alpha)$, whose corresponding distance, D_1 or D_2, is less than D^*. Note that perturbations $d\theta > 0$ and $d\theta < 0$ imply that $x_1(\alpha)$ and $x_2(\alpha)$ are on opposite sides of $x(\alpha^*)$. Let the arguments surrounding Theorem 1 be used to define a focal point z to measure the distances D_1, D_2, and D^*. Then either the pair of trajectories $x_1(\alpha)$ and $x(\alpha^*)$ or the pair of trajectories $x_2(\alpha)$ and $x(\alpha^*)$ contradicts the assertion that $x(\alpha^*)$ corresponds to a local maximum of the line integral. However, this contradiction arises from the supposition that $x(\alpha^*)$ is not a separation boundary. Therefore, we conclude that $x(\alpha^*)$ is, in fact, a separation boundary.

Apparent pathologies and other concerns

In this section, a number of subtle and potentially problematic issues related to Theorems 1 and 2 are addressed. These issues include

(1). The importance of being able to freely rotate ray $r_{N\text{-}1}$.
(2). Rays that intersect at several different points on given trajectories.
(3). Distillation regions whose boundaries are defined by multiple local maxima in distance.

In doing so, generic components are used to avoid mixture specific characteristics. We also use hypothetical residue curves whose sole attributes include only the assumptions that they are twice continuously differentiable and do not cross. In the material that follows, we show that these apparent pathologies do not affect the correctness of Theorems 1 and 2. In the accompanying illustrations, certain characteristics of residue curve maps have been exaggerated (e.g., the sizes of $B(x_0, \varepsilon_0)$ and $B(x_T, \varepsilon_T)$, the shapes and separation between adjacent trajectories, etc.) in order to highlight salient points.

The importance of freely rotating ray r_{N-1}

Note that each ray in Figure 4 intersects the pair of neighboring residue curves at one point, both trajectories are entirely contained within the cone formed by the focal point z and the rays r_0 and r_N, and the focal point lies on the convex side of all pairs of residue curves in either distillation region. In contrast, consider the residue curves shown in Figure 5, where pure component vertices A and B are saddle points, vertex C is the unstable node, and the minimum boiling azeotropic point on the hypotenuse is the stable node. For this system there are no internal boundaries. The separation boundaries are the edges of the triangular region. However, one notices immediately that there is a potential difficulty; the focal point z below the CA axis is poorly located and this causes the ray r_N (shown as a dashed line) to lie between the rays r_0 and r_{N-1} (also dashed).

There are also difficulties in measuring distances along the portions of $x_1(\alpha)$ and $x_2(\alpha)$ that lie on or below the dashed ray r_{N-1} since all rays drawn below r_{N-1} will intersect trajectories more than once. To understand this, note that from the poorly placed focal point we can measure relative distances of adjacent trajectories between the rays labeled r_0 to r_N. When we do this, trajectories closest to the CA axis are shortest. Although we know this is not correct, we cannot yet conclude there are any difficulties. However, difficulties do arise when we try to measure the remaining distances along these neighboring trajectories. To do this we must construct a secondary focal point, say z′, located anywhere on ray r_N between the original focal point and the stable node. While it is perfectly legitimate to do this, a problem occurs. When measured from z′, now trajectories closest to the CA axis are longest—instead of shortest as before. As a result, we can draw no conclusion as to which trajectory in any pair of trajectories from unstable to stable node is longest from this poorly placed focal point and its associated secondary focal point. We caution the reader not to draw incorrect conclusions regarding the arguments just presented. They do not mean that longest is not longest. They do not mean boundaries are not defined by locally longest trajectories. They simply mean that improper placements of focal points do not allow one to accurately determine the relative distances of adjacent trajectories and decide which is longest, and that's all they mean.

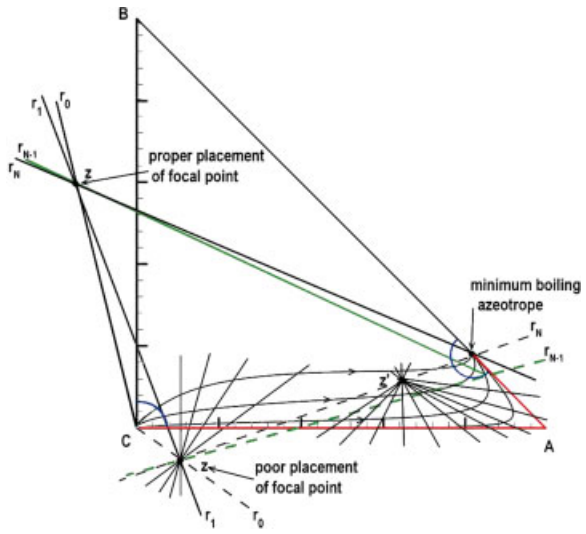

Figure 5. Importance of freely rotating ray r_{N-1}.

[Color figure can be viewed in the online issue, which is available at www.interscience.wiley.com.]

So we ask—Does this illustration represent a contradiction of Theorems 1 and 2? No! The foregoing difficulty is easily and correctly resolved by rotating the ray r_{N-1} in a clockwise direction so the focal point is properly located in the neighborhood just above the unstable node C, where rotated rays r_{N-1} and r_N are shown as solid lines in Figure 5, and so that distances along the full lengths of adjacent trajectories are calculated correctly. Note that we are free to rotate the ray r_{N-1} in the clockwise direction in order to place the focal point in the desired location using the arguments presented earlier. In particular, the point a_{1N-1} is either on or inside $B(x_T, \varepsilon_T)$ and still on the trajectory $x_1(\alpha)$—as it must be. As a result, all trajectories are now entirely contained within the cone formed by the focal point z and the rays r_0 and r_N and all rays intersect all neighboring trajectories only once. Thus Theorems 1 and 2 apply and the resulting boundary in this illustration is simply the edge CA and that portion of the hypotenuse between the stable node (i.e., minimum boiling azeotrope) and the pure component vertex A. Similar arguments hold for trajectories that initially head toward vertex B and flow down the hypotenuse toward the stable node.

Multiple intersections of rays and trajectories

It is a simple matter to construct smooth hypothetical trajectories that do not cross but have enough of a serpentine shape so that some rays intersect several trajectories multiple times. Figure 6 gives an illustration of this. Unlike the previous illustration, here the residue curves wind around in such a way that regardless of the rotation of ray r_{N-1}, several rays cut pairs of adjacent trajectories multiple times. Note that rotating r_{N-1} moves the focal point z up and to the right along the ray r_0. However, the most r_{N-1} can be rotated is governed by the intersection of r_0 with the line formed by $x_2(0)$ and the stable node, where $x_2(0)$ is given by Eq. 5. Thus the furthest to the right the focal point can be moved is shown in Figure 6 and this still results in rays that intersect trajectories multiple times. Moreover, moving the focal point down and to the left does nothing to address this difficulty. As a consequence, in situations such as this there will always be portions of adjacent trajectories on which local congruence will be reversed—potentially causing a problem with the proofs of Theorems 1 and 2. Nonetheless, this apparent

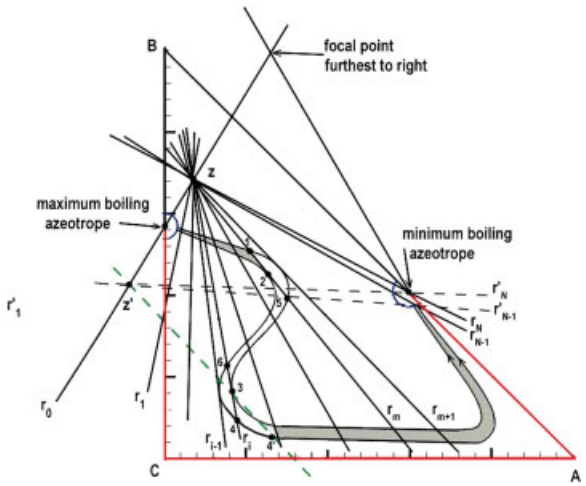

Figure 6. Multiple intersections of rays and trajectories.

[Color figure can be viewed in the online issue, which is available at www.interscience.wiley.com.]

pathology is easily resolved by constructing equal lengths of pairs of trajectories in regions where local congruence is reversed and subsequently establishing a secondary focal point to accurately calculate distances along the remaining parts of each pair of adjacent trajectories. To see this, consider Figure 6 and let the trajectory furthest from the CA axis be denoted by $x_1(\alpha)$. Let the adjacent trajectory—the one closest to the edge CA—be $x_2(\alpha)$. Also let the solid rays r_1 and r_{N-1} be constructed as shown in Figure 6, where r_{N-1} has been properly rotated slightly clockwise.

Note first that the rays r_i and r_m (as well as all rays in between) intersect either $x_1(\alpha)$ or $x_2(\alpha)$ or both multiple times. More specifically, ray r_i intersects $x_1(\alpha)$ two times and $x_2(\alpha)$ three times while the ray r_m intersect $x_1(\alpha)$ three times and $x_2(\alpha)$ two times. Note also that for those portions of $x_1(\alpha)$ and $x_2(\alpha)$ between rays r_i and r_m, local congruence is reversed when compared to those portions covered by the shaded regions between the two neighboring trajectories. Thus lengths of segments on $x_2(\alpha)$ will be smaller than lengths of segments on $x_1(\alpha)$ between rays r_i and r_m while the reverse will be true in the shaded regions. Also the distance along $x_1(\alpha)$ between rays r_m and r_{m+1} as well as the distance along $x_2(\alpha)$ between rays r_{i-1} and r_i cannot be measured by local congruence because r_{i-1} and r_{m+1} only intersect $x_2(\alpha)$ and $x_1(\alpha)$ once respectively. These distances are arcs 6–4 and 1–5 in Figure 6. Again we ask—does this illustration represent a contradiction of Theorems 1 and 2? Again the answer is no!

This is because we can still measure distances along the serpentine portions of these residue curves and compare those distances, we just cannot compare the lengths along $x_1(\alpha)$ and $x_2(\alpha)$ in this region by local congruence. Assume that the distance 1–3 along $x_1(\alpha)$ is greater than the distance 2–4 along $x_2(\alpha)$. To resolve the difficulties outlined in the previous paragraph we need to first move along $x_2(\alpha)$ from point 4 to a point say $4'$ such that the length of $x_2(\alpha)$ between points 2 and $4'$ is exactly the same as the length of $x_1(\alpha)$ between points 1 and 3. Because trajectories are smooth functions of initial conditions and do not cross, the point $4'$ along $x_2(\alpha)$ always exists. Note that it is always possible to reduce the perturbation $d\theta$ (i.e., the angle between the initial conditions for adjacent trajectories on $B(x_0, \varepsilon_0)$) so that the distance remaining along $x_2(\alpha)$ is greater than the difference between the distances of segments 1–3 and 2–4. Next, we can (and must) establish a secondary focal point z' by finding the intersection of the solid ray r_0 and the dashed line formed by the points 3 and $4'$ so that distances along each trajectory are measured accurately. Following this, we can then draw the dashed ray r_{N-1}'. With these conditions established, it is a straightforward matter to show that the total distance D_2 associated with the trajectory $x_2(\alpha)$ is greater than the total distance associated with $x_1(\alpha)$ or that $D_2 > D_1$. To see this, first note that using the focal point z, the length of $x_2(\alpha)$ is greater than the length of $x_1(\alpha)$ for the shaded region closest to the unstable node (i.e., the maximum boiling azeotrope) by local congruence. Moreover, the lengths of $x_1(\alpha)$ and $x_2(\alpha)$ (i.e., paths 1–3 and 2–$4'$) in the unshaded region are equal by construction. Thus from the unstable node to the points 3 and $4'$ respectively, it is still true that the length of $x_2(\alpha)$ is greater than the length of $x_1(\alpha)$. Now using the focal point z', it is easy to invoke local congruence to show that the length of $x_2(\alpha)$ is greater than the length of $x_1(\alpha)$ in the larger shaded region. As a result, it follows that $D_2 > D_1$. Moreover, these arguments will apply to all trajectories of this or similar serpentine shape in this region. Consequently, the resulting boundary, which in this case is comprised of the portion of the edge from the maximum boiling azeotrope to the vertex C, the entire edge CA, and the portion of the hypotenuse that runs from the vertex A to the minimum boiling azeotrope, is in fact the trajectory of maximum length.

Remarks

First, it is important for the reader to understand that the distances along $x_1(\alpha)$ and $x_2(\alpha)$ have been measured accurately. No portions of either trajectory shown in Figure 6 have been omitted or calculated more than once. Second, note that accurate measurement of relative distances along adjacent trajectories does not require the focal point to lie on the convex side of residue curves. This is clearly illustrated using the focal point z and the initial distances along $x_1(\alpha)$ and $x_2(\alpha)$ from the unstable node to points 1 and 2 respectively in Figure 6.

Distillation regions whose boundaries are defined by multiple local maxima in distance

Distillation regions whose boundaries are defined by multiple local maxima in distance are very common in ternary mixtures with multiple azeotropes. See the numerical results for the examples chloroform/methanol/acetone, ethanol/benzene/water, and methanol/acetone/methyl acetate given in Lucia and Taylor[16]. However, it is not at all obvious that Theorems 1 and 2 apply in these situations. The reason is this. For these types of distillation regions, trajectories can be highly curved near either the stable or unstable node or both—sometimes spanning the full range of angles for the associated balls that define feasible initial or terminus conditions. Figure 7 gives an illustration of this, where the distillation region shown has two boundaries defined by trajectories

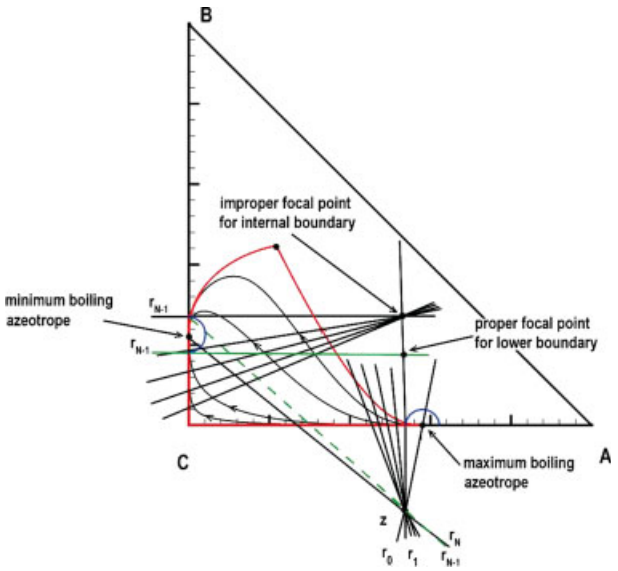

Figure 7. Distillation regions with multiple local maxima in distance.

[Color figure can be viewed in the online issue, which is available at www.interscience.wiley.com.]

of maximum length—one that runs from the maximum boiling azeotrope to the vertex C to the minimum boiling azeotrope along the edges of the feasible region, and the other which is the internal boundary that passes through the saddle point azeotrope shown in the figure.

Note also that around the unstable node (i.e., the maximum boiling azeotrope) all residue curves leave $B(x_0, \varepsilon_0)$ essentially in the direction of vertex C. Thus, the ray r_1 is a line with a positive slope just slightly less than infinity. On the other hand, in the neighborhood of the stable node (i.e., the minimum boiling azeotrope) the trajectories enter everywhere it is feasible. That is, they cover $B(x_T, \varepsilon_T)$ from $-\pi/2$ to $\pi/2$. For the lower portion of this distillation region in the neighborhood of the boundary defined by edges (i.e., where trajectories entering $B(x_T, \varepsilon_T)$ at or near an angle of $-\pi/2$), there are no difficulties. The ray r_{N-1} is the lower horizontal line, the corresponding focal point is just above the unstable node—as shown in Figure 7, and Theorems 1 and 2 assert that the boundary comprised of edges is in fact given by the line integral of local maximum length.

On the other hand, for the upper portion of this region where the boundary is an internal boundary and several trajectories enter at angle of approximately $\pi/2$, the ray r_{N-1} is the upper horizontal line. Unfortunately this leads to the ray r_N being located between rays r_{N-1} and r_1. As described earlier, this gives ambiguity in measuring distances. However, straightforward clockwise rotation of the ray r_{N-1} (such that r_{N-1} passes through both trajectories under consideration and the point a_{1N-1} is inside $B(x_T, \varepsilon_T)$) resolves this difficulty, again as described in previous discussions. Consequently, the focal point can be moved so that it actually lies below the feasible region and no ambiguities arise in measuring relative distances accurately. The result is that the internal distillation boundary correctly corresponds to the trajectory of local maximum distance.

Consider a related subtle issue with regard to accurately measuring distances. If a given distillation region has boundaries defined by two distinctly different trajectories of local maxima distance, then by continuity there must be a trajectory of minimum distance somewhere in between. Clearly we have shown that proper focal points can be selected in order for Theorems 1 and 2 to apply in the neighborhood of the true boundaries in this illustration. However, what about in the neighborhood of the trajectory of shortest distance—where focal points must change more abruptly? Does a region such as this represent a contradiction to Theorems 1 and 2? Again the answer is no! Arguments very similar to those already presented in this section can be used to easily resolve this difficulty as well.

Additional considerations

It is neither possible nor necessary to present results for all conceivable generic residue curve maps for ideal and nonideal ternary mixtures to conclude that separation boundaries correspond to line integrals of local maximum length. To see this, note that residue curve maps for ideal and nonideal zeotropic ternary mixtures always have separation boundaries that correspond to edges of the triangular region. Furthermore, these situations are covered by Figures 5 and 6—despite the manner in which the individual trajectories wind around within the feasible region. On the other hand, Kiva et al.[21] discuss generic residue curve maps for various classifications of ternary azeotropic mixtures due to earlier workers in the field. For example, Figure 21 in Kiva et al. shows the 26 classifications of residue curve maps for ternary azeotropic mixtures according to Serafimov[22]. However, close examination of these diagrams in the context of the material presented in this article clearly shows that all topological structures exhibit behavior that is qualitatively similar to that described by Figures 4, 5, 6, and/or 7 within any given distillation region—regardless of the number of distillation regions. Consequently, it is straightforward to conclude that Theorems 1 and 2 apply to all structures in the Serafimov classification and therefore that separation boundaries for ternary azeotropic mixtures are defined by locally longest line integrals from any given unstable node to all reachable stable nodes. Finally, we note that Theorems 1 and 2 apply to distillation boundaries for equilibrium or kinetically controlled reactive separation systems provided there are two degrees of freedom (see, Taylor et al.[23]).

Conclusions

In this article, rigorous proof of the fact that separation boundaries for ternary liquid mixtures are characterized by local maxima in the line integral from any unstable node to all reachable stable nodes was given. Our analysis is valid for ideal and nonideal mixtures and uses only the assumptions that residue curves are at least twice continuously differentiable and do not cross. The proofs that were presented are based on some simple geometric concepts—local congruence, which must hold for any pair of adjacent residue curves in the limit, and the existence of focal points that can measure distance correctly. Several potential pathological situations were discussed to show that they have no bearing on the validity of the proofs—irrespective of the way in which

trajectories wind around the feasible region. Our analysis was also shown to apply to the classification of ternary azeotropic mixtures due to Serafimov.

The natural progression of this work is its extension to mixtures with larger numbers of components. For example, the numerical work of Bellows and Lucia[17] illustrates that the optimization concepts used to characterize separation boundaries in ternary systems readily extends to mixtures with four or more component. In particular, Bellows and Lucia illustrate that separation boundaries for four component mixtures correspond to local maxima in surface areas subject to Levi-Civita parallelism and, in doing so, use the nonlinear programming approach given in Lucia and Taylor[16] to actually construct these surfaces of maximum area. However, the proofs given in this article cannot be directly applied to four component mixtures because they do not consider parallel transport. Thus some additional considerations will be necessary to prove similar results for four component mixtures.

We close by drawing a connection between this work and other research on distillation lines and the energy efficiency of distillation separations. First, for the most part everything we have said about residue curve maps and boundaries also carries over to distillation lines at total reflux and boundaries. By distillation lines at total reflux we mean rectifying and stripping lines of the form

$$x'_j = [(r+1)/r]y_j - x_j - (1/r)x_{\mathrm{D}} \tag{14}$$

$$x'_j = [(s)/(s+1)]y_j - x_j + [1/(s+1)]x_{\mathrm{B}} \tag{15}$$

where r and s are the reflux ratio and stripping (or reboil) ratio respectively, x_{D} and x_{B} are the distillate and bottoms compositions, and the subscript j denotes the jth stage. At total reflux, it is easy to see that that last term in Eqs. 14 and 15 drops out and both equations become equivalent to the residue curve given by Eq. 4. However, there is one important difference; the step size h for distillation lines at total reflux is assumed to be $h = 1$. This step size has some impact on approximating distillation boundaries with distillation lines at total reflux (or reboil). Inaccuracies in integration from using a step size of $h = 1$ can prevent one from actually using a reflux or reboil ratio near infinity. It can happen that for very large values of reflux or reboil ratio and a step size of $h = 1$, Eqs. 14 and 15 result in compositions that are outside the feasible region. Thus some flexibility must be permitted in these cases and perhaps the use of the phrase distillation lines at maximum reflux or reboil is more accurate.

Having said this, it is possible to conclude that distillation boundaries correspond to distillation lines at maximum reflux and reboil that have local maximum length. In addition, it is also true that distillation lines that approximate boundaries correspond to the highest energy consumption for the given separation.

Acknowledgments

The authors would like to thank the National Science Foundation for support of this work under Grant No. CTS-0624889. AL would also like to thank Ms. Leah Octavio and Mr. Amit Amale for producing the graphical illustrations in this article.

Literature Cited

1. Ostwald W. Dampfdrucke ternarer gemische. Abahndlungen der mathematisch-physischen der konig sachsischen. *Gesellschaft der Wissenschaften*. 1900;25:413.
2. Ostwald W. Lehrbuk der allgemetnen chemie. Leipzig: Engelmann, 1902.
3. Schreinemakers FAH. Dampfdrucke ternarer gemische. I. Theoretischer teil. *Z Phys Chem*. 1901;36:257–289.
4. Schreinemakers FAH. Dampfdrucke ternarer gemische. II. Theoretischer teil. *Z Phys Chem*. 1901;36:413–449.
5. Schreinemakers FAH. Dampfdrucke ternarer gemische. III. Theoretischer teil. *Z Phys Chem*. 1901;36:711–740.
6. Barbosa D, Doherty MF. The influence of chemical reactions on vapor-liquid phase diagrams. *Chem Eng Sci*. 1988;43:529–540.
7. Barbosa D, Doherty MF. The simple distillation of homogeneous reactive mixtures. *Chem Eng Sci*. 1988;43:541–550.
8. Barbosa D, Doherty MF. Design and minimum reflux calculations for single-feed multicomponent reactive distillation columns. *Chem Eng Sci*. 1988;43:1523–1537.
9. Pham HN, Doherty MF. Design and synthesis of heterogeneous azeotropic distillations. *Chem Eng Sci*. 1990;45:1823–1836.
10. Pham HN, Doherty MF. Design and synthesis of heterogeneous azeotropic distillations. *Chem Eng Sci*. 1990;45:1837–1843.
11. Slaughter DW, Doherty MF. Calculation of solid-liquid equilibrium and crystallization paths for melt crystallization processes. *Chem Eng Sci*. 1995;50:1679–1694.
12. Fien G-JAF, Liu YA. Heuristic synthesis and shortcut design of separation processes using residue curve maps: a review. *Ind Eng Chem Res*. 1994;33:2505–2522.
13. Peterson EJ, Partin LR. Temperature sequences for categorizing all ternary distillation boundary maps. *Ind Eng Chem Res*. 1997;36:1799–1811.
14. Rooks RE, Julka V, Doherty MF, Malone MF. Structure of distillation regions for multicomponent azeotropic mixtures. *AIChE J*. 1998;44:1382–1391.
15. Pöpken T, Gmehling J. Simple method for determining the location of distillation region boundaries in quaternary systems. *Ind Eng Chem Res*. 2004;43:777–783.
16. Lucia A, Taylor R. The geometry of separation boundaries. I. Basic theory and numerical support. *AIChE J*. 2006;52:582–594.
17. Bellows ML, Lucia A. The geometry of separation boundaries—four component mixtures. *AIChE J*. 2007;53:1770–1778.
18. Doherty MF, Perkins JD. On the dynamics of distillation processes. I. The simple distillation of multicomponent, nonreacting homogeneous mixtures. *Chem Eng Sci*. 1978;33:281–301.
19. Hurewicz W. Lectures in ordinary differential equations. Cambridge, MA: MIT Press, 1958.
20. Taylor AE, Mann WR. Advanced Calculus. Lexington, MA: Xerox College Publishing, 1972.
21. Kiva VN, Hilmen EK, Skogestad S. Azeotropic phase equilibrium diagrams: a survey. *Chem Eng Sci*. 2003;58:1903–1953.
22. Serafimov LA. The azeotropic rule and the classification of multicomponent mixtures. VII. Diagrams for ternary mixtures. *Russian J Phys Chem*. 1970;44:567–642.
23. Taylor R, Miller A, Lucia A. The geometry of separation boundaries: systems with chemical reaction. *Ind Eng Chem Res*. 2006;45:2777–2786.

Manuscript received Dec. 8, 2006, and revision received Apr. 6, 2007.